Science of the Total Environment 848 (2022) 157527

Contents lists available at ScienceDirect

Science of the Total Environment

journal homepage: www.elsevier.com/locate/scitotenv

Identifying the dominant impact factors and their contributions to heatwave events over mainland China

Liaofeng Liang [a,b,1], Linfei Yu [a,b,1], Zhonggen Wang [a,c,*]

[a] Key Laboratory of Water Cycle and Related Land Surface Processes, Institute of Geographic Sciences and Natural Resources Research, Chinese Academy of Sciences, Beijing 100101, China
[b] University of Chinese Academy of Sciences, Beijing 101400, China
[c] National Institute of Natural Hazards, Ministry of Emergency Management of China, Beijing 100085, China

HIGHLIGHTS

- A large difference is found between 1960–1984 and 1985–2019 for various heatwave metrics over the mainland China.
- At the junction region of C, N, and SW, the change of heatwave is less evident than that of other regions.
- According to MLR results, the factors of climate change show the highest explanatory rates for heatwaves over China.
- For heatwave frequency, urbanization is the dominant factor in NE, EA, and QT, with RC ranging from 32.8 % to 38.9 %.

GRAPHICAL ABSTRACT

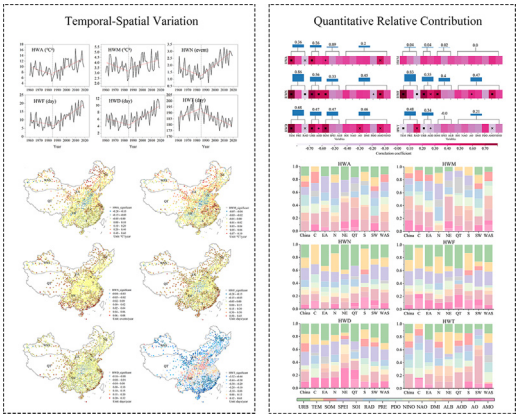

ARTICLE INFO

Editor: Martin Drews

Keywords:
Heatwaves
Spatial-temporal variation
Impact factors
Contribution quantification

ABSTRACT

The heatwave frequency and intensity have significantly changed as the climate warms and human activities increase, which poses a potential risk to human society. However, the impact factors that determine the change of heatwave events remain unclear. Here, we estimated the heatwave events based on data from 2474 in-suit gauges during 1960–2018 at daily scale in China. Besides, we explored possible drivers and their contributions to the change of heatwave based on correlation analysis, multiple linear regression (MLR), and random forest (RF) in different subregions of China. The results show that the temporal changes of all heatwave metrics exhibit significant differences between the period 1960–1984 and the period 1985–2019. Spatially, the heatwave frequency and duration significant increase in the southern China (S), eastern arid region (EA), northeastern China (NE), Qinghai-Tibet region (QT) and western arid and semi-arid region (WAS). The occurrence of the first heatwave event in a year tends to be earlier in S, NE, EA, WAS, and QT than before. Based on the regression modelling and RF, human activities play an important role in heatwave intensity in all subregions of China. For heatwave frequency, urbanization generate a dominant influence in NE, EA, and QT, with relative contributions (RC) ranging from 32.8 % to 38.9 %. Long-term climate change exerts the dominant influence in C, N, and S. Moreover, the first day of the yearly heatwave event (HWT) in NE is significantly influenced by climate change, with RC of 33.9 % for temperature variation (TEM). Our findings could

* Corresponding author.
E-mail address: wangzg@igsnrr.ac.cn (Z. Wang).
[1] These authors contributed equally.

http://dx.doi.org/10.1016/j.scitotenv.2022.157527
Received 19 April 2022; Received in revised form 9 July 2022; Accepted 16 July 2022
Available online 2 August 2022

provide critical information for understanding the causes of heatwave across different regions of China in the context of rapid urbanization and climate change.

1. Introduction

As kind of extreme disaster, a heatwave is usually regarded as a durative period that the temperature exceeding a prescribed threshold (Dong et al., 2021; Li, 2020). Extreme heatwaves have a largely negative influence on the human health, the social economy development, and the natural ecosystem (Coumou and Rahmstorf, 2012; Xu et al., 2018; Xu et al., 2016). For example, a heatwave across European caused >70,000 deaths during the summer in 2003 (Robine et al., 2008). Similarly, an unprecedented heatwave resulted in nearly 55,000 excess deaths, which occurred in Western Russia and Moscow in 2010 (Barriopedro et al., 2011). A northwest Atlantic heatwave significantly affected biological habitats and biodiversity in 2012, leading to a considerable destruction of natural nutrient cycles (Mills et al., 2013). Nevertheless, heatwaves have increased in frequency, intensity, and duration all over the world due to enhanced global warming in recent decades (Mukherjee and Mishra, 2021). Rohini et al. (2016) indicated that the frequency of heatwaves has increased by one incident per two decades, and their length has increased by 2 days per decade in northwest India. Meanwhile, heatwaves have been more frequent and longer in Europe and southeast Asia, which poses a threat to physically active humans (Casanueva et al., 2020; Pogačar et al., 2018). Besides, previous studies also indicated that the severe heatwave intensity is growing at a quick rate around the world such as Australia's southern areas (Jyoteeshkumar et al., 2021), northern and central Thailand (Huang et al., 2018), and North America (Mondal and Mishra, 2021).

Climate change and anthropogenic forcing are widely regarded as the primary causes of heatwave occurrence (Kang and Eltahir, 2018). Specifically, global rise in mean temperature and radiation can lead to an increase in the frequency of heatwaves (Intergovernmental Panel on Climate, 2014). Previous studies have commonly demonstrated that human activities such as urbanization accounts for the rise in heatwaves across China, and its contribution is still increasing over time (Liao et al., 2018). The main reason of the urbanization effect is the increases in impervious surfaces, which results in more solar energy being absorbed in urban regions (Athukorala and Murayama, 2021). Besides, atmospheric modes also play a significant role in heatwave formation by modulating the background climate, including the El Niño-Southern Oscillation (ENSO) (Luo and Lau, 2019) and the Atlantic Multidecadal Oscillation (AMO) (Horton et al., 2015). Changes in the physical properties of clouds and atmospheric aerosols also have a great impact on the radiative balance, which may affect local and circulation air temperature (Lyamani et al., 2006). And some land surface properties, such as soil moisture and natural surface albedo, are also highly associated with high temperatures (Stegehuis et al., 2021). Linking with latent heat flux, the soil moisture can regulate the net radiation budget (Alexander, 2011) and the albedo always impacts the surface energy balance to influence the temperature (Seo et al., 2021). Overall, the causes of heatwaves and their physical mechanisms are complicated, and however, our current understanding of the dominant factors in heatwaves is still limited due to the complexity of the dominant impact variables and their relationship with heatwaves.

In general, the heatwaves can be estimated by different metrics, including the intensity, frequency, duration, etc., which depend on the application sections. For instance, the public health scholars tend to pay more attention on the heatwave intensity (Sun et al., 2014; Xu et al., 2019), whereas the agricultural sections are concerned more about the onset time, frequency and duration of heatwave (He et al., 2022; Lobell et al., 2012). Therefore, it is of great significance to carry out a comprehensive evaluation of different heatwave metrics (including intensity, frequency, duration, and occurrence time) for their applications in various industries. Although some studies have ever explored the relative contributions of some impact factors to heatwaves, including climate change (Clark et al., 2010), atmospheric circulation (Clark and Brown, 2013) and anthropogenic activities (Vautard et al., 2020), while they more focused on the relationship between some drivers and a single heatwave aspect (Perkins-Kirkpatrick et al., 2017; Wu et al., 2012). Consequently, a deeply study for the relationship between different heatwave metrics and impact factors can greatly help us underatand the causes of heatwave in the future.

Due to rapid urbanization and climate change, heatwaves have swept across China since the mid-1980s with significantly increasing frequency and strength (Liu et al., 2021b; Wang et al., 2019). From 1951 to 2006, the average surface temperature over China increased by about 1.35 °C (Piao et al., 2010), and the summer heatwave has grown significantly in area and frequency since the 1990s (Ye et al., 2014). Moreover, the heatwave in southeast China induced massive economic damage and caused a total loss of 4.20 billion U.S. dollars in 2013 (Xia et al., 2018). Therefore, it is of practical significance to improve our understanding of spatiotemporal variations and the driving factors of heatwaves in China. This study aims at addressing two scientific issues: 1) how is the space-time changes characteristics of heatwave based on various evaluation metrics across mainland China? 2) what are the main drivers and their relative contributions (RC) to heatwave in China?

2. Data

2.1. Study area

The study area includes mainland China, where summer temperatures are consistently high across the country. During winter, the temperature difference between north and south is significant, with the temperature decreasing as moving from south to north (Duan et al., 2021). Besides, the precipitation in China tends to reduce from the southeast area to the northwest inland, with more precipitation in summer (L. Yu et al., 2021; Y. Yu et al., 2021). China has a diverse topography that includes plateaus, hills, basins, plains, and deserts, which also have different climatic types. Therefore, a widely konwn climatic sub-regions classification is used in this study (Shen et al., 2021), including the central China (C), the eastern arid region (EA), the northern China (N), the northeastern China (NE), the Qinghai-Tibet region (QT), the southern China (S), the southwestern China (SW), and the western arid and semi-arid region (WAS) (Fig. S1).

2.2. Observation data from 1960 to 2019

The ground observations from 2474 national stations are used in this study. The Resource and Environment Science and Data Center (https://www.resdc.cn/) provides the data for 70 summer seasons (June to September) from 1950 to 2019. The raw data is quality-checked through the conventional quality control procedures of the National Meteorological Information Center (NMIC), such as the climatological limit check, the station or regional extremes check, the internal consistency check, the temporal and geographic consistency checks, etc. (Xu et al., 2013). All gauges are tested the homogenization by the PMTred and PMFred algorithm, which is based on the penalized maximal t test (PMT) and the penalized maximal F (PMF) (Wang et al., 2007). Based on the homogeneity test results, we also use quantile-matching algorithm (QM) to adjust the uneven station data. Since many stations do not cover the period 1950–1959, the measurements from 1960 to 2019 are utilized to identify the heatwave in this study. A gauge is considered missing if it has five or more missing days in any summer season and a total of 1906 stations are remained after checking. The missing segment, which have less than five missing days, is filled by linear interpolation method. The annual and warm season (June to September) average temperature are shown in Figs. S2 and S3, respectively.

2.3. Impact factors data

We selected fifteen potential drivers from 1985 to 2018 in this study, including monthly temperature (TEM), monthly precipitation (PRE), downward shortwave radiation (RAD), urbanization (URB), aerosol optical depth (AOD), soil water (SOM), standardized precipitation-evapotranspiration index (SPEI), surface albedo (ALB), Niño 3.4 index (NINO), Southern Oscillation Index (SOI), Dipole Mode Index (DMI), North Atlantic Oscillation index (NAO), Arctic Oscillation index (AO), Atlantic Multi decadal Oscillation index (AMO), and Pacific Decadal Oscillation index (PDO). Besides, in order to compare the effects of climate change, antropogenic activities, land surface processes, and atmospheric circulation, the impact factors are divided into four categories (Wang et al., 2022; Wu et al., 2021).

The monthly PRE and TEM are calculated based on the observation data during 1950–2019 from the Resource and Environment Science and Data Center. The monthly AOD, ALB, SOM, and RAD data are obtained from the MERRA-2 reanalysis dataset (https://gmao.gsfc.nasa.gov/reanalysis/MERRA-2/). The MERRA-2 reanalysis dataset has been widely evaluated and validated in previous studies around the world (Fei and Wang, 2019; Hua et al., 2019). Particularly, Wang et al. (2020) validated MERRA-2 albedo dataset with sun photometers over eastern China and found that the accuracy of the MERRA-2 albedo is acceptable in eastern China. For SOM, the accuracy of MERRA-2 (unbiased RMSE of 0.053 $m^3\ m^{-3}$) is higher than that of ERA-Interim/Land and MERRA (Reichle et al., 2017). For RAD, Zhou et al. (2020) reported that the overall correlation coefficient between the surface radiation and the MERRA-2 monthly radiation product is 0.9. Notably, due to the length limitation of MERRA-2 and SPEI data sets, the analysis of HW potential drivers can only be conducted in the common period of 1980 to 2018. Similarly, due to the limited availability of data, the period 1985–2018 was chosen to calculate the relative contribution (RC) of driving factors in this study.

The impervious surface area can be regarded as a measure of urbanization (Zhang et al., 2020). The 30 m annual land cover data is used in this study (Yang and Huang, 2021). The SPEI is adopted to depict seasonal drought conditions in this work, which is developed by the Spanish National Research Council (CSIC) with a resolution of 0.5° × 0.5° (https://spei.csic.es/spei_database/). The data sources of atmospheric circulation indices are summarized in Table S1, including of NINO, SOI, IOD, NAO, AO, AMO, and PDO. Generally, the preceding soil water is an influential driver of the HW and the average Nino3.4 index of the previous winter can define the El Nino event (Luo and Lau, 2019). Therefore, the antecedent soil moisture (February–May) and the Nino 3.4 index of the previous winter are calculated. The other impact factors are analyzed by the average from June to September of each year.

3. Method

3.1. Definition and metrics of heatwave

The excess heat factor (EHF) is used to identify heatwave in this study (Perkins and Alexander, 2013). EHF, which is calculated using climatology and the previous 30 day mean temperature, has the advantage of considering both historical averages and current situations. It has been widely adopted to identify heatwave in previous studies (Perkins et al., 2012; Wondmagegn et al., 2021). Two indices to calculate EHF are as follows:

$$EHI_{\mathrm{sig}} = \frac{T_{m_i} + T_{m_{i-1}} + T_{m_{i-2}}}{3} - T_{m_{90i}} \tag{1}$$

$$EHI_{acc} = \frac{T_{m_i} + T_{m_{i-1}} + T_{m_{i-2}}}{3} - \frac{T_{m_{i-3}} + \cdots + T_{m_{i-32}}}{3} \tag{2}$$

where T_m is daily average value of maximum and minimum temperature, with the *i* indicating the relevant day and days prior. EHI_{sig} is the difference between the previous 3 day mean and the climatological 90th percentile for the time period 1960–2019, and EHI_{acc} is the difference between the previous 3 day mean and the preceding 30 day mean. Then the EHF is calculated by:

$$EHF = EHI_{\mathrm{sig}} \times \max\left(1, EHI_{\mathrm{acc}}\right) \tag{3}$$

The unit of the EHF index is in $^{\circ}C^2$ and the positive values of EHF represent heatwave-like conditions for the day *i*. If EHF is consecutivly greater than zero for three or more days, a heatwave event is identified to onset.

Based on the criteria above, this study examines the different heatwave features based on six metrics. Specifically, HWM is the average daily magnitude across all heat wave events within a year. HWA is the EHF of the hottest day (or peak) of the hottest yearly event. HWN is the yearly number of heat waves. HWD is the length (in days) of the longest yearly event. HWF is the sum of participating heatwave days per year that satisfy the definition criteria. HWT is the first day of the first yearly heatwave event.

3.2. Change trend detection

In this study, the Mann–Kendall (MK) trend test (Kendall, 1957; Mann, 1945) and Theil–Sen median slope (Sen, 1968; Theil, 1992) are adopted to analyze the change trend. A further procedure called trend-free pre-whitening (TFPW) is used to eliminate the influence of autocorrelation on the MK test (Yue, 2002). The TFPW consists of four steps: (i) estimating the Sen's slope on the original data; (ii) removing the trend to obtain a detrended time series; (iii) removing the lag-1 autocorrelation on to generate a detrended pre-whitened time series; and (iv) adding the trend back to generate the processed time series. In TFPW-MK test, the calculation method of standardized test statistic Z is as follows:

$$Z = \begin{cases} \dfrac{S-1}{\sqrt{Var(S)}} & S > 0 \\ 0 & S = 0 \\ \dfrac{S+1}{\sqrt{Var(S)}} & S < 0 \end{cases} \tag{4}$$

where S is the Mann–Kendall statistic (S). If Z value is positive, it signifies an upward trend and if negative, it indicates a decreasing trend. Trends are tested using a two-tailed test with a significance level α. When $|Z| > Z_{1-\alpha/2}$ ($Z_{1-\alpha/2}$ is the standard normal deviation), a significant trend exists. Significance level of 0.05 is used in this study.

3.3. Correlation and explanatory rates

The Pearson's correlations between the potential influence factors and heatwave indicators are calculated to assure significant relationships between factors and heatwave metrics. The multiple linear regression (MLR) is used to estimate the explanatory rates of four categories, including climate change, anthropogenic activities, land surface processes, and atmospheric circulations. Therefore, for each heatwave metric, we performed 4 MLR runs on an annual time step over 1985–2018. In MLR, the following models are constructed:

$$Y_i = b + a_1 x_{i1} + a_2 x_{i2} + \ldots a_p x_{ip} + \xi_i \tag{5}$$

where ξ_i is a prediction residual corresponding to the *i*th data sample. The ordinary least squares method is applied to estimate the value of the intercept *b* and coefficients a_i and to minimize the sum of squared residuals $\Sigma_{i=1}^{n}\xi_i^2$.

3.4. Variable screening methods

Before evaluating the RC, a variable selection procedure is carried to find the vital variables, which can therefore greatly improve the performance of the model (Blanchet et al., 2008; Xiong et al., 2020). Stepwise multiple linear regression (SMLR) can be used with data sets that have non-normal distributions, and it can be expanded to more generalized models. The main goal of this approach is to identify effective variables through calculating the Akaike

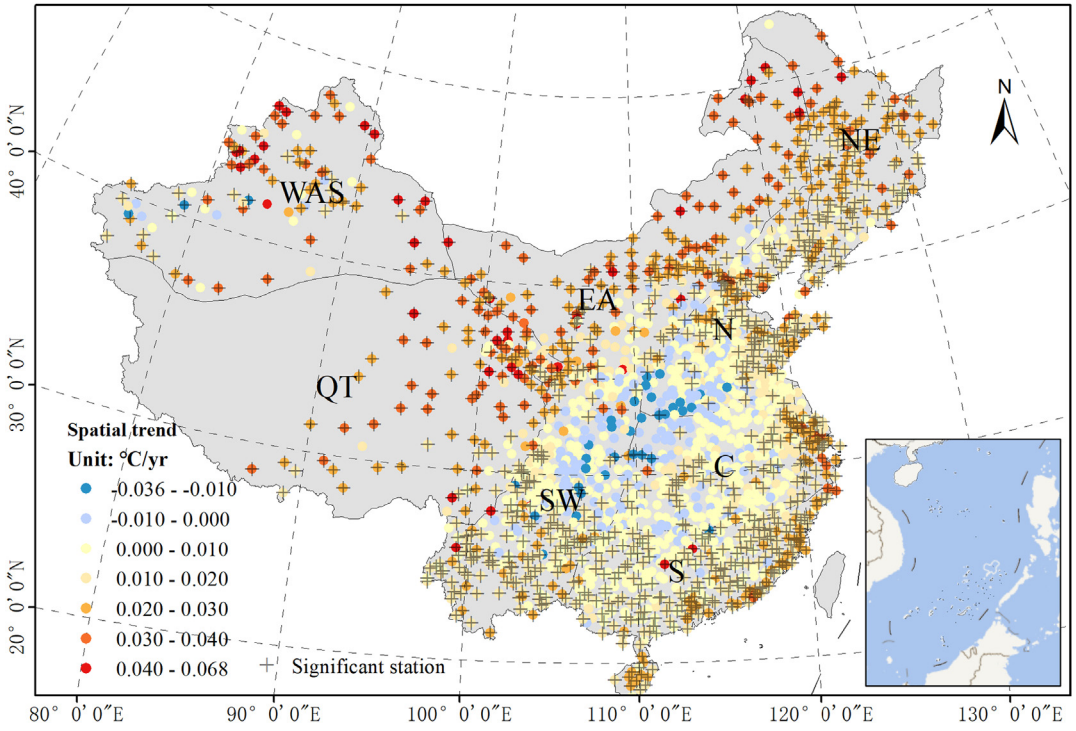

Fig. 1. The trend of warm season temperature for each gauge across China during 1960–2019. The cross indicates the change trend is significant at 0.05 level.

information criterion (AIC) after filtering potential unrelated predictors. Details of SMLR can be found in Yamashita et al. (2007).

In this study, a combination of SMLR and randomforest (RF) is conducted to identify the valid correlative variables for heatwave. First, each factor is ranked by SMLR and RF, which can obtain two rank scores. Second, two rank scores are summed up to get the total score for each factor. Finally, for ensuring that there is at least one driving factor in each category (climate change, antropogenic activities, land surface processes, and atmospheric circulation), the leading eight factors that have the smallest total score are selected as input driving factors for heatwaves and used to calculate the contributions.

3.5. Evaluating the RC of drivers

RF has the advantage of considering split candidates from a randomly selected portion of the original feature set, which results in decorrelated trees and lower variance (Belgiu and Drăguţ, 2016). RF is widely used in assessing the importance of independent variables (Luo et al., 2020; Yu and Leng, 2022). The mean decline in Gini (MDG) has been used as a statistical tool to evaluate the relative significance of the variables based on an out-of-bag data term. There are 54 RF models (6 metrics × 9 regions) for RC evaluation and in each RF model we choose eight factors as input variables, which are selected by the variables screening method above. The

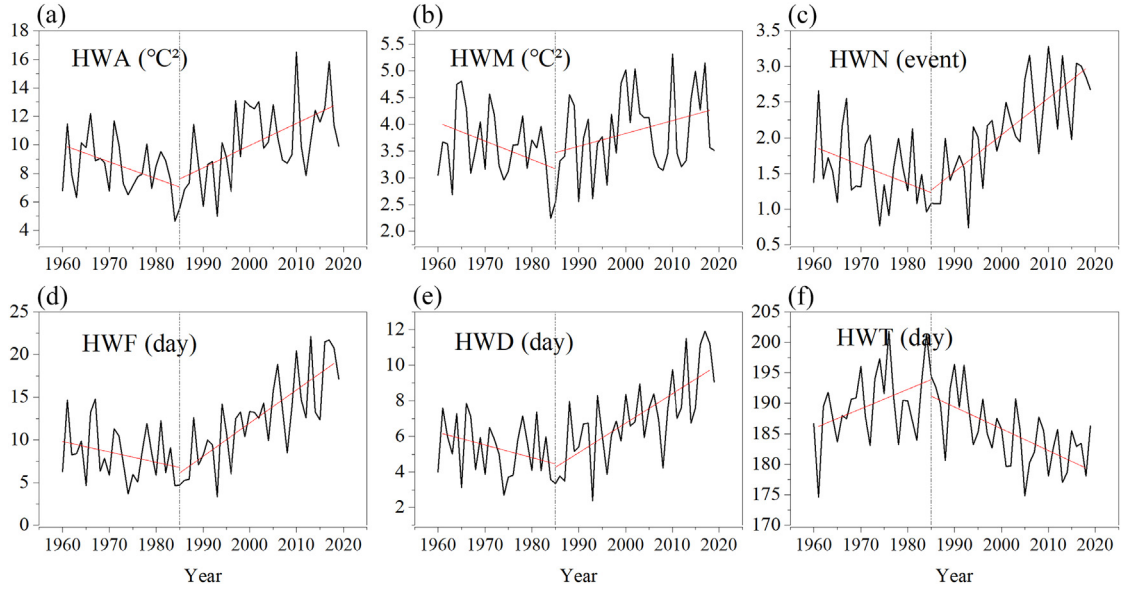

Fig. 2. Temporal changes of HWA (a), HWM (b), HWN (c), HWF (d), HWD (e) and HWT (f) over China during 1960–2019. The red lines are the linear fits to the data and the dash black line is the year of 1985.

details on model training and validation are provided in the supplement. The RC are calculated as follows:

$$\mu = \frac{MDG}{\Sigma_1^i MDG} \times 100\% \quad (6)$$

where i represents the number of input factors, μ is the RC of each factor, and MDG represents the mean decrease of Gini purity.

In terms of the data scale, the point-to-pixel analysis method is adopted to match the series HW metrics data, which are calculated by temperature gauges, with the corresponding pixels of gridded drivers data. Only pixels in which at least one ground-based gauge can be selected and used for the calculation (Sharifi et al., 2018). When the stations are included within the pixels, the abstraction of pixels is processed directly based on the locations of temperature gauges. However, if the temperature gauge locates on near the corner of four pixels or the edge between two pixels (<0.01° off the edge), the average value of four or two pixels around the gauge is utilized as the basis for calculation. Additionally, because the RC analysis is conducted at station scale, this method avoids the influence of different product spatial resolutions on the evaluation results.

4. Results

4.1. Temporal trends of temperature and heatwave

The warm season temperature trends of all gauges are presented in Fig. 1. Overall, the maximum, minimum, and average trends are 0.068, −0.036, and 0.014 °C/year, respectively. The temperature shows an increasing trend in 54.4 % stations, with the highest of 0.068 °C/year and the lowest of 0.005 °C/year. By contrast, the decreasing temperature trends range from −0.036 to −0.011 °C/year. Spatially, the positive trends are mainly over S, NE, WAS and QT, occupying the stations amount of 70.2 %, 92.7 %, 72.8 %, and 82.3 %, respectively. Particularly, the temperature trends in central China are remarkably lower than in other regions, with 28.1 % of gauges showing increasing trends. In addition, for N and SW, the temperature trends exhibited a significant spatial heterogeneity

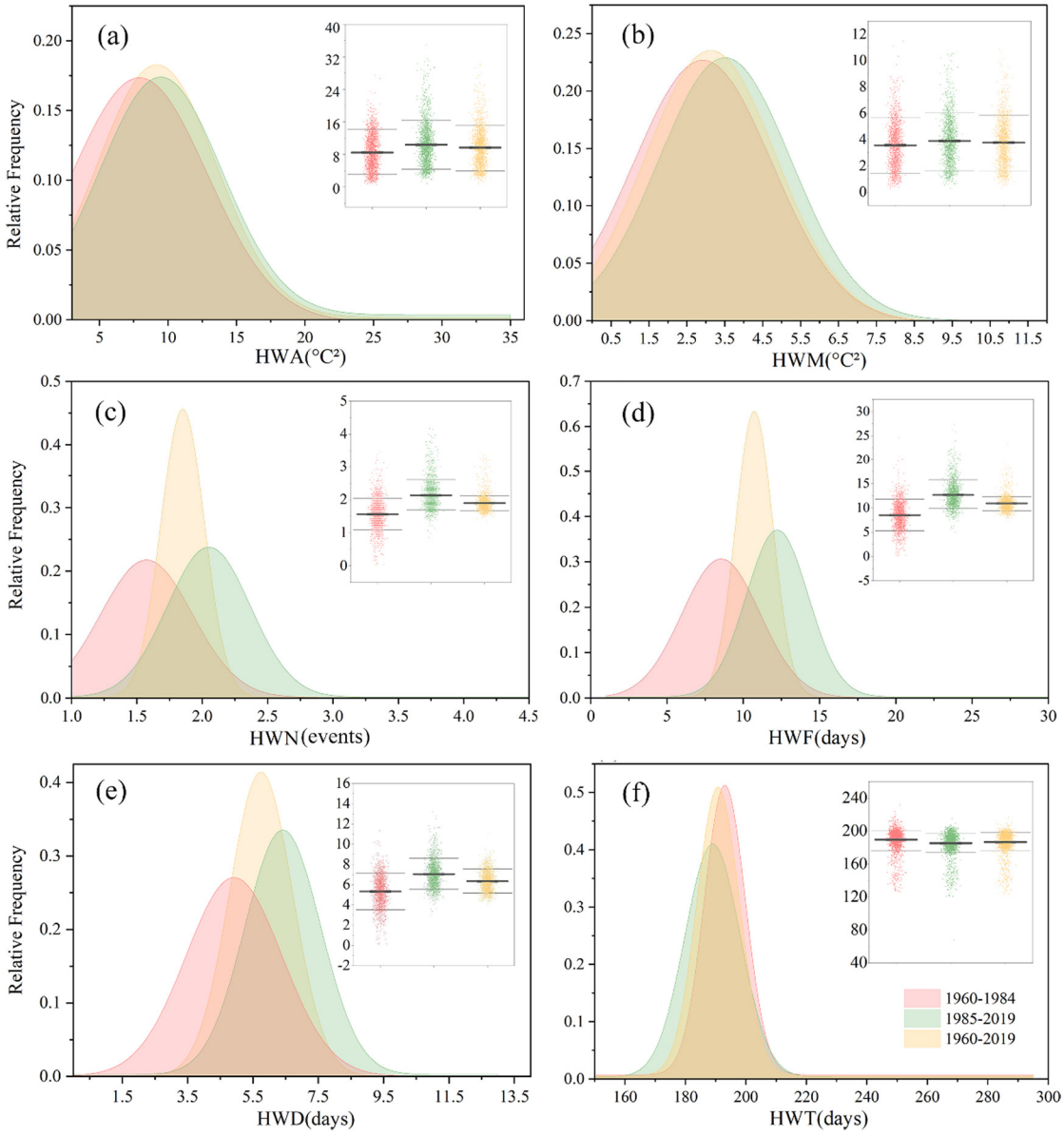

Fig. 3. The probability distribution of metrics in all stations during 1960–1985 (red), 1986–2019 (green) and 1960–2019 (yellow). The distributions are fitted by Gauss curve and optimized by the Levenberg-Marquardt method. The embedded dot plots indicate the corresponding distribution of heatwave metrics in all stations and the black lines indicate three intervals (75 %, 50 %, and 25 %).

of south-north pattern and the percentages of positive stations in two regions are 39.4 % and 42.1 %, respectively.

From Fig. 2, the six metrics show different change directions from the period of 1960–1984 to 1985–2019. The year 1985 is generally used as a change date in previous study about the characters of extreme temperature and precipitation over China (W. Gao et al., 2021; X. Gao et al., 2021; Zheng et al., 2019).To reveal the temperal change of HW trend, we also divide the 1960–2019 into two periods (1960–1984 and 1985–2019) in the analysis of HW charaters. In the HW characters analysis in this study, the year 1985 can be used to divide the whole period into two periods due to the opposite trends. Specifically, the frequency, duration, and intensity of heatwaves decrease slightly while the HWT increased during 1960 to 1984 (Fig. 2a). However, after 1985, the values of all metrics significantly increase, especially for HWN (Fig. 2c), HWF (Fig. 2d), and HWD (Fig. 2e). During 1985 to 2019, the trends for HWN, HWF, and HWD are 0.05 event/year, 0.39 day/year, and 0.17 day/year, respectively. Besides, the HWT decreases significantly, and the first heatwave of a year tended to occur 0.36 day earlier per year during the period 1985–2019.

Fig. 3 shows the probability density distribution of heatwave metrics in all stations during the periods 1960–1984, 1985–2019, and 1960–2019. In addition to HWT, the mean values of HWA, HWM, HWN, HWF, and HWD during 1985–2019 are higher than those of 1960–1984 (Fig. 3a–e), with an average of 10.37 °C^2, 3.90 °C^2, 2.13 events, 12.66 days, and 7.04 days, respectively. For HWN, HWF, and HWD, the distribution curve is more homogeneous during 1960–1984 (Fig. 3c–e), suggesting that the values become more concentrated and more stations have higher heatwave frequency after 1984. For HWT, the station average for 1985–2019 is 4.39 days less than that of 1960–1984 (Fig. 3f).

4.2. Spatial patterns of heatwave metric trends

Spatially, the trends of six metrics of observation stations are shown in Fig. 4. Overall, all metrics present a non-significant ($p > 0.05$) change at the junction region of C, N, and SW, which includes parts of the north China plain and the Sichuan basin. The increasing trends of HWA are mainly found in the S, C, EA, QT and WAS, which occupy the stations amount of 38.2 %, 44.3 %, 30.7 %, 37.5 %, and 31.5 %, respectively (Fig. 4a). The HWN, HWF, and HWD of S, EA, NE, QT, and WAS also exhibit a significant increasing trend (Fig. 4c–e). Particularly, the increasing HWM trends in S and C are more common than those of other regions with 31.7 %

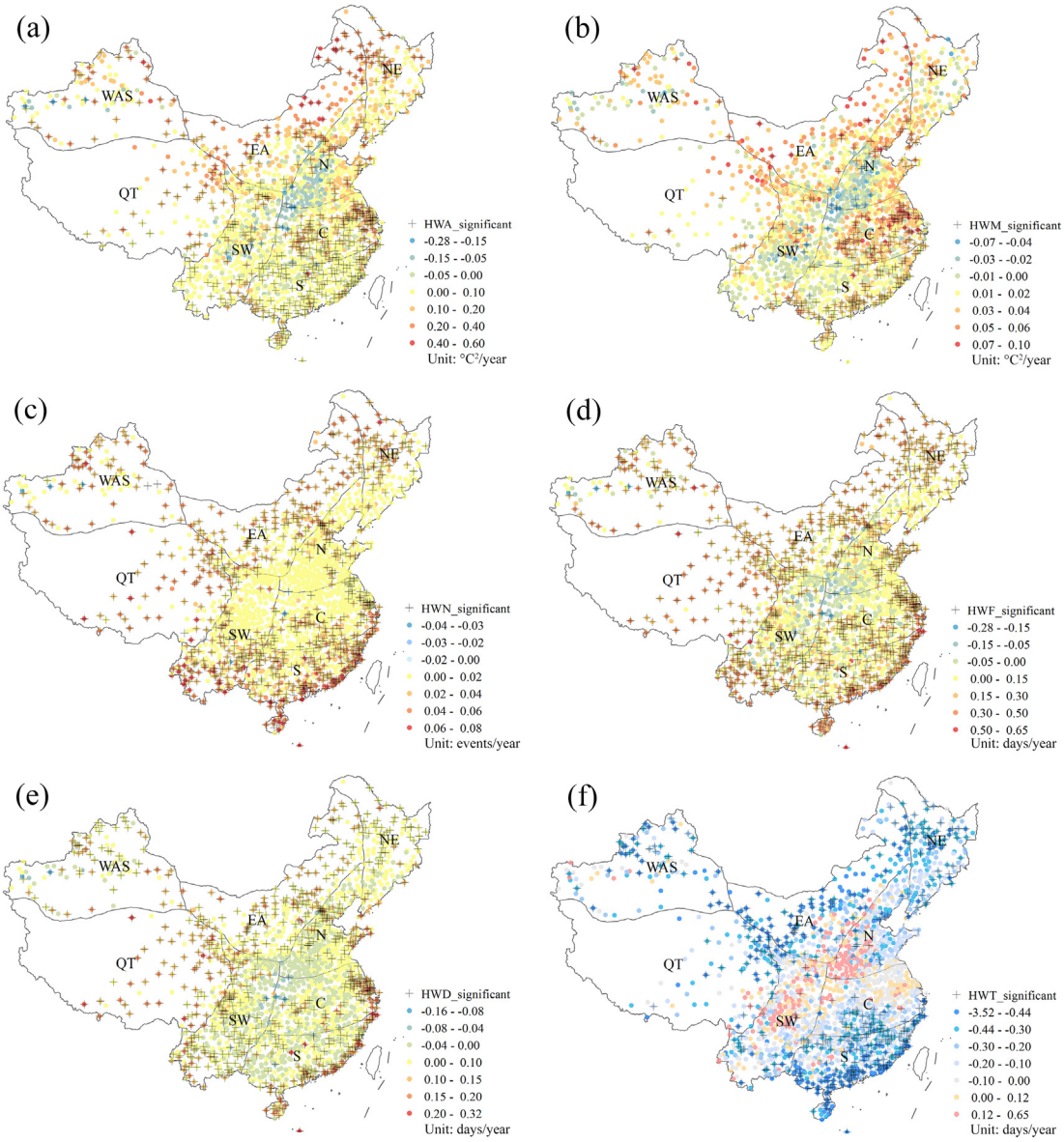

Fig. 4. The trends of HWA (a), HWM (b), HWN (c), HWF (d), HWD (e) and HWT (f) at each station over China from 1960 to 2019. The cross represents significance at 0.05 level.

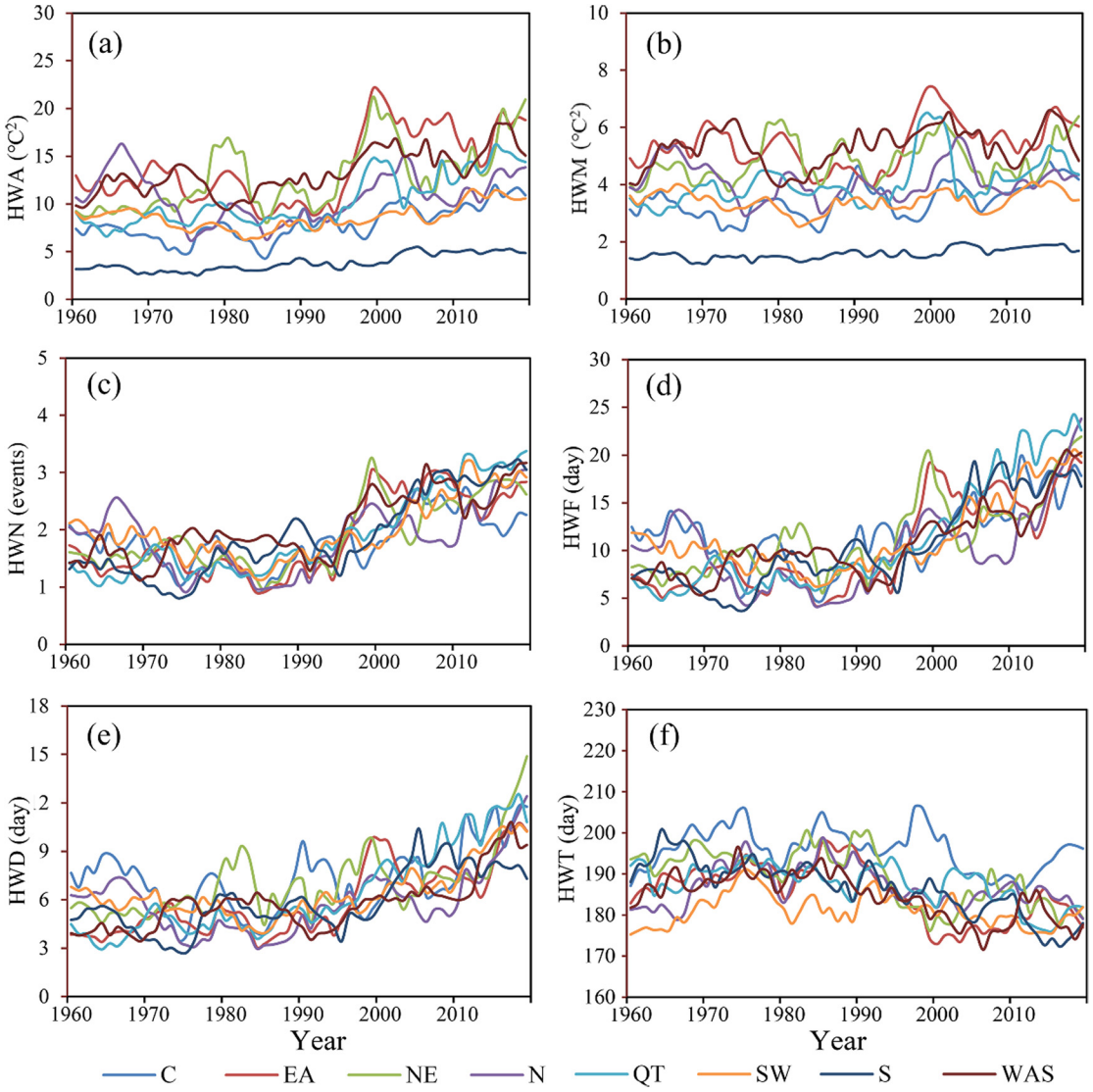

Fig. 5. The temporal change of HWA (a), HWM (b), HWN (c), HWF (d), HWD (e) and HWT (f) in different subregions during 1960–2019 based on sliding 5-year window.

and 24.7 % stations, respectively (Fig. 4b). And the HWT values decrease significantly in all subregions except for N, C, and SW (Fig. 4f). In addition, we also investigated the frequency and duration of heatwaves in QT and find that there were 37.5 %, 69.8 %, 78.1 %, 76.0 %, and 31.2 % of stations with a significant increase for HWA, HWN, HWF, HWD, and HWT, respectively.

The temporal variations of six heatwave metrics in all subregions are shown in Fig. 5. For HWN, HWF, and HWD (Fig. 5c–e), the positive trends are found in different subregions during 1960–2019. The HWT tend to decrease in all subregions except for C after 1990 (Fig. 5f). However, for HWA and HWM, the differences between subregions are larger than other metrics (Fig. 5a and b). Specifically, the HWA in S, SW, and C have smoother fluctuations than other regions, with smaller standard deviations of 0.87, 1.27, and 1.80 °C^2, respectively. The same phenomenon is also found in the HWM of S and C, with standard deviations of 0.20 and 0.36 °C^2.

4.3. Relationship between HW and driving factors

The correlation analysis results of fifteen variables and MLR explanatory rates (adjust R^2) for four variable categories over mainland China are shown in Fig. 6. For HWA, HWN, HWF, and HWD, the climate factors show the highest explanatory rates among four categories, with values of 36 %, 86 %, 83 %, and 68 %, respectively (Fig. 6a, c–e). On the other hand, the land surface process factors have the lowest explanatory rates (9 %, 33 %, 40 %, and 47 %) among the four categories for HWA, HWN, HWF, and HWD. Only one factor (SOM) of land surface processes significantly correlates with all heatwave metrics except for HWM. The anthropogenic activities have significant positive relationships with HWA, HWN, HWF, and HWD. Besides, HWT is negatively correlated with TEM, URB, AOD, and AMO (with correlation coefficients of −0.72, −0.62, −0.43, and −0.53) (Fig. 6f). All correlation coefficients in HWM are unsignificant ($p > 0.05$), and the explanatory rates of four categories for HWM are minimal (Fig. 6b). In addition, Fig. S5–S6 presents the correlation analysis and MLR results in C, EA, N, NE, QT, S, SW and WAS. The frequency and duration of heatwave are dominated by the factors of climate change.

4.4. Contributions of dominant drivers in different subregions

Based on SML and RF models, the importance of different variables to heatwave metrics is quantified, and the input variables for RC evaluation are shown in Table S2. For all heatwave metrics in EA, N, NE, QT, and S, the AO, URB, SPEI, and AOD are regarded as the explanatory variables in RC analysis. Based on RF, the RC of each variable in different subregions are exhibited in Fig. 7. For HWA and HWM in EA, N, NE, SW, and WAS, the RC of URB range from 6.8 % to 21.0 % (Fig. 7a and b). Meanwhile, for HWA and HWM, the RC of SPEI range from 9.7 % to 25.1 % and the

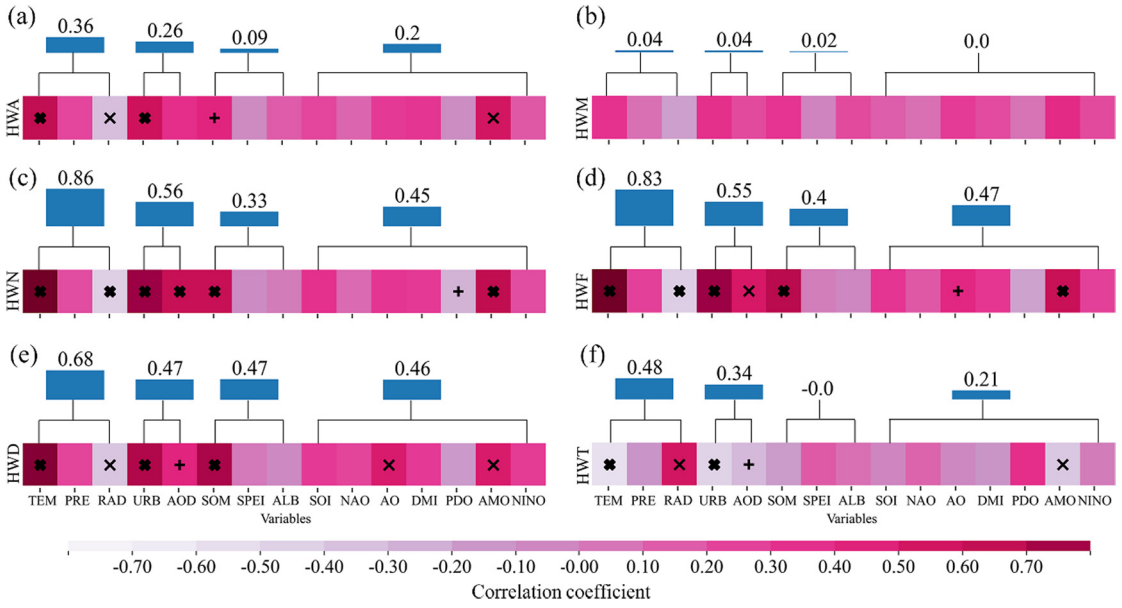

Fig. 6. The correlation coefficient between variables and the metrics over mainland China. The blue columns denote the explanatory rates of MLR results for four variables categories (climate change, anthropogenic activities, land surface processes and atmospheric circulation, respectively). "+", "x", and bold "x" represent the statistical significance at 0.05, 0.01 and 0.001, respectively.

RC of AOD range from 11.5 % to 38.0 %, respectively. In particular, AOD is the main explanatory variable for HWA and HWM in NE, with RC of 29.6 % and 38.0 %. For HWN and HWF, URB presents a dominant influence, with RC ranging from 32.8 % to 38.9 % in NE, EA and QT (Fig. 7c and d). In C, N, and S, the RC of TEM for HWN and HWF range from 25.9 % to 32.2 %. Compared to other heatwave metrics, HWD is mainly regulated by AO, URB, and SPEI, and the AO exerts a great influence (RC of 31.4 %) on the HWD in NE (Fig. 7e). For HWT, TEM has a RC of 33.9 % in NE and AOD have a dominant influence on heatwave onset time in SW (Fig. 7f) with the RC of 42.9 %.

5. Discussion

This study analyzes the changes in heatwave across mainland China using station-observed temperatures from 1960 to 2019. Overall, consistent with previous studies (Liao et al., 2018; Shi et al., 2021), most areas of China show increasing heatwave frequency and duration during 1985–2019. This study found that climate change shows a large influence on heatwave, which is physically reasonable because warming climate usually aggravates extreme hot events over a large spatial scale (Guo et al., 2017; Liu et al., 2021a). Similarly, the SPEI also acts as a crucial driver for heatwave frequency, duration, and onset time, because the land-atmosphere coupling favors the amplification of hot spells and leads to mega-heatwaves (Geirinhas et al., 2021). Moreover, the dry conditions can amplify heat entrainment from the top of the atmospheric boundary layer and enhance the near-surface heat storage (Miralles et al., 2014). The source of surface humidity includes both moisture advection and area evaporation, which generally increases the probability of HW (An et al., 2020). For SOM, the increase of temperature is always regarded as the standard response to low soil moisture (Herold et al., 2016). However, because an increasing sensible heat flux to the atmosphere can compensate the decreasing latent heat flux, the effect of low SOM also cannot cause the increase of HW metrics (Alexander, 2011). During 1985–2018, the agricultural land, wetlands and lakes in China has been widely shifted to urban land, which cause a significant perturbation to surface energy balance (Zhou and Chen, 2018). The albedo of some urban land decrease and store more radiation energy, which contribute to the occurrence of HW (Zhao et al., 2014). Besides, the increasing aerosols enhance the transfer of solar radiation energy and reduce the diurnal temperature difference, which result in a local insulation effect and attribute to the occurrence of HW (Wild et al., 2007). The local and remote aerosol emission changes can impact the summer extreme temperature event by inducing precipitation-soil moisture-cloud-temperature feedback (Dong et al., 2016). The increase of urban impervious surface (URB) also makes the surface albedo increase, which leads to a high relative contribution to HW. In addition to land surface process, this study also presents the significant relationship between atmospheric circulation and heatwave metrics in different regions. For example, AO is a critical atmospheric circulation factor for heatwave duration over China, which is regarded as an important climatic driver for the East Asian by affecting the westerly wind and the Siberian high (He et al., 2017). Through causing eastward propagating Rossby wave trains toward Eurasia, AMO change is also considered as an important contributor to heatwave frequency (Zhou and Wu, 2016). Through Atlantic-Eurasian teleconnection, the Atlantic SSTs always influence the high temperature events in northern China (Deng et al., 2019). And positive AMO can cause the circulation anomalies, which warm parts of China and increase HW frequency (Choi et al., 2020). Furthermore, the low-frequency PDO dynamics can result in a persistent and continuous atmosphere boundary condition, which influences the regional climate and potentially contributes to the land temperature (Vijverberg and Coumou, 2022). In this study, PDO has a significant relationship with HWF in C, which is consistent with Guo et al. (2020).

Spatially, in C, S, EA, NE, and WAS, the heatwave frequency and duration increase significantly from 1960 to 2019. The positive trends in heatwave intensity are mainly located in the southern area, where the Western Pacific Subtropical High has a huge impact. Specifically, the extension of the Western Pacific Subtropical High can cause an unusual sinking of the airflow and relatively low humidity, both of which are expected to raise air temperatures in the lower troposphere of south China (Chen and Lu, 2015), causing the area more susceptible to heatwaves than other areas on average. On the other hand, from the spatial change patterns of the different heatwave metrics, the heatwave change at the junction region of C, N, and WS is less evident than that of other regions, which might due to that the region is influenced both by the Western Pacific Subtropical High and the cold waves from north (L. Yu et al., 2021; Y. Yu et al., 2021). Besides, summertime shifts of the Asian jet stream toward the equator, as well as changes in stratospheric temperatures, may induce surface temperatures in the junction region to cool (Wang et al., 2013). Furthermore, increased aerosols and cloudiness restrict solar radiation, producing additional cooling in the junction region throughout the day (Chen and Zhai, 2017).

Previous studies have already quantified the contributions of climate change and urbanization in some subregions of China, such as the North

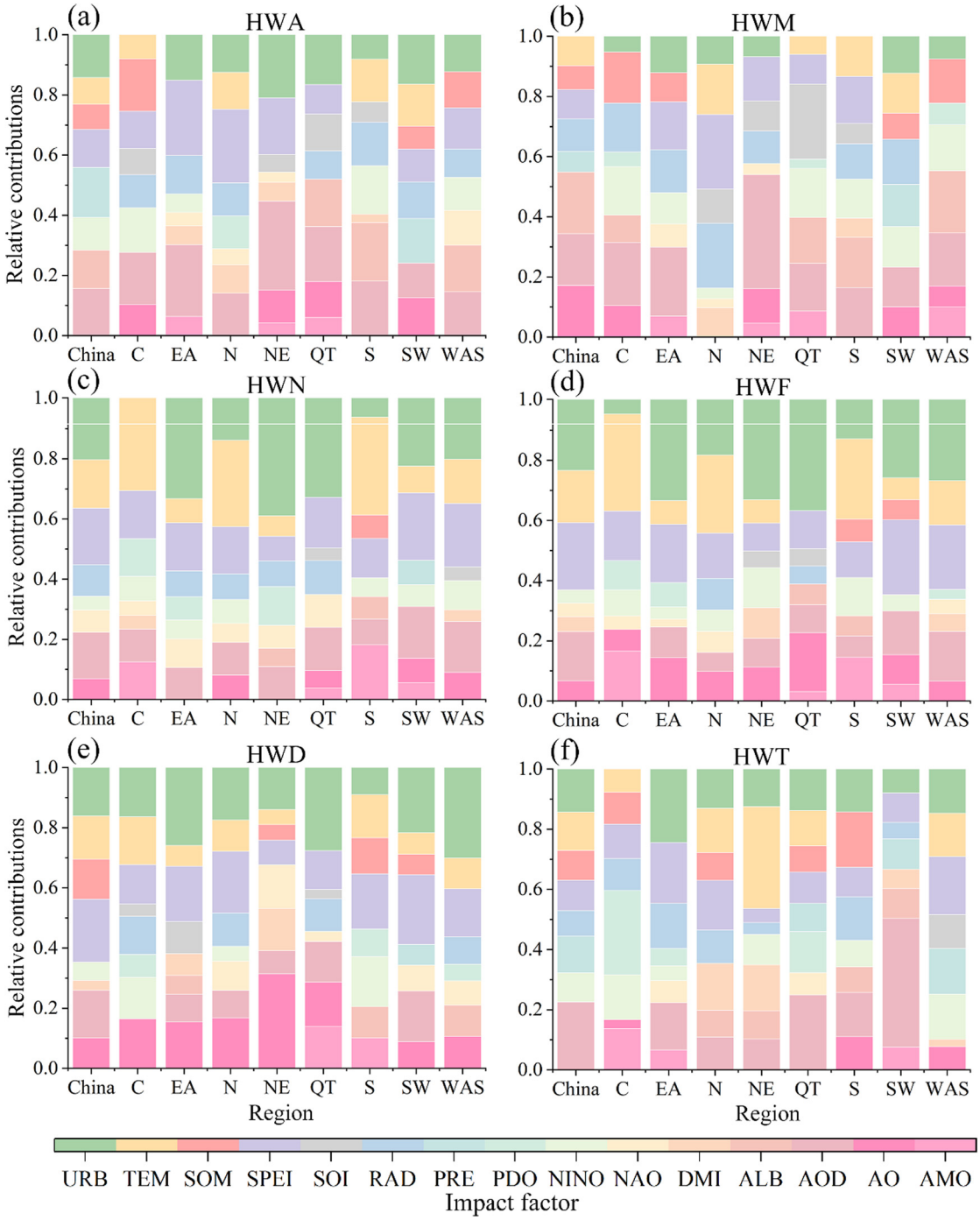

Fig. 7. The relative contributions (RC) of impact factors to the HWA (a), HWM (b), HWN (c), HWF (d), HWD (e) and HWT (f) in different subregions of China during 1985–2018.

China plain (Kong et al., 2020). This study complemented the series of recent studies at station scale and demonstrates the widespread potential for anthropogenic activities and climate change to exacerbate all metrics of heatwave from 1985 to 2018. Compared to previous studies, we emphasized the differences in drivers' contributions in different subregions. For instance, urbanization plays a dominant role in the heatwave frequency and duration of QT, EA, and NE (Fig. 7c–d). Taking QT as an example, since 1960, China's rapid economic development has resulted in a continual growth in the plateau's population (Qi et al., 2020). From 1990 to 2019, Tibet's population has increased from 2.18 million to 3.51 million people (Liu et al., 2021a, 2021b; S. Liu et al., 2021). Due to the rising population and rapidly developing tourism, the urbanization rate in Tibet is also continually increasing, although it is still slower than in other parts of China (W. Gao et al., 2021; X. Gao et al., 2021). Besides, the sedentarization of the historically nomadic peoples also result in significant increasing in settlements and roads area (Lu et al., 2009). Since 1985, the increasing urban land has drastically reduced forest cover on the Qinghai-Tibetan Plateau, particularly in its eastern regions (Luo et al., 2020).

In this study, the heatwave metrics are derived from ground-based observations of temperature, and thus they do not rely on any parameter assumptions like the remote sensing reanalysis data. However, it should be emphasized that the observation-derived results can be impacted by the distribution and quality of weather stations. Therefore, heatwave metrics and contribution results may have limitations in areas with few or uneven meteorological stations. For instance, since the observation stations of QT are mostly distributed in the eastern area of Qinghai-Tibet plateau, the

analysis results can only represent the situation in the eastern area (Fig. S1). Further studies of mechanisms are needed to explain the more concrete relationships between individual and combinations of HW drivers. Besides, MERRA-2 reanalysis dataset, have difficulty simulating some climate variables, such as low-level clouds and their corresponding cloud radiation effects. Although comprehensively validated, the MERRA-2 reanalysis dataset, especially for ALB and RAD data, still contains certain uncertainties and errors, which are expected to be reduced through better design and development of satellite missions and retrieval algorithms.

6. Conclusion

In this study, we estimated the change trends of heatwave during 1960–2019 and the relative contributions of impact factors to six heatwave metrics during 1985–2018. The main findings are as follows:

1) The warm season temperature has exhibited a significant ($p < 0.05$) positive trend in most stations from 1960 to 2019, with a maximum trend of 0.068 °C/year. Spatially, the trends in central China have mostly exhibited a decreasing tendency. For HWA, HWM, HWN, HWF, and HWD, there are negative trends from 1960 to 1984, and after 1985, the trends become positive.
2) For different subregions of China from 1960 to 2019, six heatwave metrics present non-significant ($p > 0.05$) change at the junction regions of C, N, and SW. The heatwave frequency and duration increase significantly in S, EA, NE, QT, and WAS. In addition to N, C, and SW, the station HWT significantly decreases.
3) Overall, the climate factors present the highest explanatory rates among four categories, while the land surface process has the lowest explanatory rates for HWA, HWN, HWF, and HWD during 1985 to 2018. Human activities have significant positive relationships with HWA, HWN, HWF, and HWD.
4) Based on RF, anthropogenic activities have a dominant contribution to heatwave intensity in all subregions from 1985 to 2018. Besides, for heatwave frequency (HWN and HWF), urbanization has a major influence in NE, EA, and QT, ranging from ranging from 32.8 % to 38.9 %. In C, N, and S, the long-term climate change has a great contribution on HW frequency, ranging from 25.9 % to 32.2 %. Heatwave duration is mainly regulated by AO, URB, and SPEI.

CRediT authorship contribution statement

Liaofeng Liang: Conceptualization, Methodology, Software, data curation, Writing-Original draft preparation.

Linfei Yu: Conceptualization, Methodology, Writing-Original draft preparation, Writing-review and editing.

Zhonggen Wang: Conceptualization, Supervision, Funding acquisition.

Declaration of competing interest

The authors declare that they have no known competing financial interests or personal relationships that could have appeared to influence the work reported in this paper.

Acknowledgements

This study was financially supported by the Second Tibetan Plateau Scientific Expedition and Research Program (STEP) (No. 2019QZKK0903), the Strategic Priority Research Program of the Chinese Academy of Sciences (No. XDA23040104).

Appendix A. Supplementary data

Supplementary data to this article can be found online at https://doi.org/10.1016/j.scitotenv.2022.157527.

References

Alexander, L., 2011. Extreme heat rooted in dry soils. Nat. Geosci. 4 (1), 12–13. https://doi.org/10.1038/ngeo1045.

An, N., Dou, J.J., Gonzalez-Cruz, J.E., Bornstein, R.D., Miao, S.G., Li, L., 2020. An observational case study of synergies between an intense heat wave and the urban Heat Island in Beijing. J. Appl. Meteorol. Climatol. 59 (4), 605–620. https://doi.org/10.1175/jamc-d-19-0125.1.

Athukorala, D., Murayama, Y., 2021. Urban heat island formation in greater Cairo: spatio-temporal analysis of daytime and nighttime land surface temperatures along the urban–rural gradient. Remote Sens. 13 (7), 1396. https://doi.org/10.3390/rs13071396.

Barriopedro, D., Fischer, E.M., Luterbacher, J., Trigo, R.M., García-Herrera, R., 2011. The hot summer of 2010: redrawing the temperature record map of Europe. Science 332 (6026), 220–224. https://doi.org/10.1126/science.1201224.

Belgiu, M., Drăguţ, L., 2016. Random forest in remote sensing: a review of applications and future directions. ISPRS J. Photogramm. Remote Sens. 114, 24–31. https://doi.org/10.1016/j.isprsjprs.2016.01.011.

Blanchet, F.G., Legendre, P., Borcard, D., 2008. Forward selection of explanatory variables. Ecology 89 (9), 2623–2632. https://doi.org/10.1890/07-0986.1.

Casanueva, A., Kotlarski, S., Fischer, A.M., Flouris, A.D., Kjellstrom, T., Lemke, B., Nybo, L., Schwierz, C., Liniger, M.A., 2020. Escalating environmental summer heat exposure—a future threat for the European workforce. Reg. Environ. Chang. 20 (2), 1–14. https://doi.org/10.1007/s10113-020-01625-6.

Chen, R., Lu, R., 2015. Comparisons of the circulation anomalies associated with extreme heat in different regions of eastern China. J. Clim. 28 (14), 5830–5844. https://doi.org/10.1175/jcli-d-14-00818.1.

Chen, Y., Zhai, P., 2017. Revisiting summertime hot extremes in China during 1961–2015: overlooked compound extremes and significant changes. Geophys. Res. Lett. 44 (10), 5096–5103. https://doi.org/10.1002/2016gl072281.

Choi, N., Lee, M.I., Cha, D.H., Lim, Y.K., Kim, K.M., 2020. Decadal changes in the interannual variability of heat waves in East Asia caused by atmospheric teleconnection changes. J. Clim. 33 (4), 1505–1522. https://doi.org/10.1175/jcli-d-19-0222.1.

Clark, R.T., Brown, S.J., 2013. Influences of circulation and climate change on European summer heat extremes. J. Clim. 26 (23), 9621–9632. https://doi.org/10.1175/Jcli-D-12-00740.1.

Clark, R.T., Murphy, J.M., Brown, S.J., 2010. Do global warming targets limit heatwave risk? Geophys. Res. Lett. 37 (17). https://doi.org/10.1029/2010gl043898.

Coumou, D., Rahmstorf, S., 2012. A decade of weather extremes. Nat. Clim. Chang. 2 (7), 491–496. https://doi.org/10.1038/nclimate1452.

Deng, K.Q., Yang, S., Ting, M.F., Zhao, P., Wang, Z.Y., 2019. Dominant modes of China summer heat waves driven by Global Sea surface temperature and atmospheric internal variability. J. Clim. 32 (12), 3761–3775. https://doi.org/10.1175/jcli-d-18-0256.1.

Dong, B.W., Sutton, R.T., Highwood, E.J., Wilcox, L.J., 2016. Preferred response of the east asian summer monsoon to local and non-local anthropogenic sulphur dioxide emissions. Clim. Dyn. 46 (5–6), 1733–1751. https://doi.org/10.1007/s00382-015-2671-5.

Dong, Z., Wang, L., Sun, Y., Hu, T., Limsakul, A., Singhruck, P., Pimonsree, S., 2021. Heatwaves in Southeast Asia and their changes in a warmer world. Earth's Future 9 (7). https://doi.org/10.1029/2021ef001992.

Duan, R., Huang, G., Li, Y., Zheng, R., Wang, G., Xin, B., Tian, C., Ren, J., 2021. Ensemble temperature and precipitation projection for multi-factorial interactive effects of GCMs and SSPs: application to China. Front. Environ. Sci. 9, 382. https://doi.org/10.3389/fenvs.2021.742326.

Fei, F., Wang, K., 2019. Does the modern-era retrospective analysis for research and applications-2 aerosol reanalysis introduce an improvement in the simulation of surface solar radiation over China? Int. J. Climatol. 39 (3).

Gao, X., Li, T., Sun, D., 2021. Regional differentiation regularity and influencing factors of population change in the Qinghai-Tibet Plateau, China. Chin. Geograph. Sci. 31 (5), 888–899. https://doi.org/10.1007/s11769-021-1223-7.

Gao, W., Duan, K., Li, S., 2021. A spatial–temporal analysis of cold surge days in northern China during 1960–2016. Nat. Hazards 108 (1), 147–162. https://doi.org/10.1007/s11069-021-04659-z.

Geirinhas, J.L., Russo, A., Libonati, R., Sousa, P.M., Miralles, D.G., Trigo, R.M., 2021. Recent increasing frequency of compound summer drought and heatwaves in Southeast Brazil. Environ. Res. Lett. 16 (3), 034036. https://doi.org/10.1088/1748-9326/abe0eb.

Guo, E., Wang, Y., Bao, Y., 2020. Assessing spatiotemporal variation of heat waves during 1961–2016 across mainland China. Int. J. Climatol. 40 (6), 3036–3051. https://doi.org/10.1002/joc.6381.

Guo, X., Huang, J., Luo, Y., Zhao, Z., Xu, Y., 2017. Projection of heat waves over China for eight different global warming targets using 12 CMIP5 models. Theor. Appl. Climatol. 128 (3), 507–522. https://doi.org/10.1007/s00704-015-1718-1.

He, S., Gao, Y., Li, F., Wang, H., He, Y., 2017. Impact of Arctic oscillation on the east asian climate: a review. Earth Sci. Rev. 164, 48–62. https://doi.org/10.1016/j.earscirev.2016.10.014.

He, Y., Fang, J., Xu, W., Shi, P., 2022. Substantial increase of compound droughts and heatwaves in wheat growing seasons worldwide. Int. J. Climatol. https://doi.org/10.1002/joc.7518.

Herold, N., Kala, J., Alexander, L.V., 2016. The influence of soil moisture deficits on Australian heatwaves. Environ. Res. Lett. 11 (6), 8. https://doi.org/10.1088/1748-9326/11/6/064003.

Horton, D.E., Johnson, N.C., Singh, D., Swain, D.L., Rajaratnam, B., Diffenbaugh, N.S., 2015. Contribution of changes in atmospheric circulation patterns to extreme temperature trends. Nature 522 (7557), 465–469. https://doi.org/10.1038/nature14550.

Hua, W.J., Zhou, L.M., Nicholson, S.E., Chen, H.S., Qin, M.H., 2019. Assessing reanalysis data for understanding rainfall climatology and variability over central equatorial Africa. Clim. Dyn. 53 (1–2), 651–669. https://doi.org/10.1007/s00382-018-04604-0.

Huang, C., Cheng, J., Phung, D., Tawatsupa, B., Hu, W., Xu, Z., 2018. Mortality burden attributable to heatwaves in Thailand: a systematic assessment incorporating evidence-based lag structure. Environ. Int. 121 (Pt 1), 41–50. https://doi.org/10.1016/j.envint.2018.08.058.

<collab>Intergovernmental Panel on Climate, C.collab, 2014. Climate Change 2013 – The Physical Science Basis: Working Group I Contribution to the Fifth Assessment Report of the Intergovernmental Panel on Climate Change. Cambridge University Press, Cambridge https://doi.org/10.1017/CBO9781107415324.

Jyoteeshkumar, P., Perkins-Kirkpatrick, S.E., Sharples, J.J., 2021. Intensifying Australian heatwave trends and their sensitivity to observational data. Earth's Future 9 (4), e2020EF001924. https://doi.org/10.1029/2020ef001924.

Kang, S., Eltahir, E.A., 2018. North China plain threatened by deadly heatwaves due to climate change and irrigation. Nat. Commun. 9 (1), 1–9. https://doi.org/10.1038/s41467-018-05252-y.

Kendall, M.G., 1957. Rank correlation methods. Biometrika 44, 298. https://doi.org/10.2307/2333282.

Kong, D., Gu, X., Li, J., Ren, G., Liu, J., 2020a. Contributions of global warming and urbanization to the intensification of human-perceived heatwaves over China. J. Geophys. Res.-Atmos. 125 (18). https://doi.org/10.1029/2019jd032175.

Li, X., 2020. Heat wave trends in Southeast Asia during 1979–2018: the impact of humidity. Sci. Total Environ. 721, 137664. https://doi.org/10.1016/j.scitotenv.2020.137664.

Liao, W., Liu, X., Li, D., Luo, M., Wang, D., Wang, S., Baldwin, J., Lin, L., Li, X., Feng, K., Hubacek, K., Yang, X., 2018. Stronger contributions of urbanization to heat wave trends in wet climates. Geophys. Res. Lett. 45 (20), 11310–11317. https://doi.org/10.1029/2018gl079679.

Liu, J., Ren, Y., Tao, H., Shalamzari, M.J., 2021a. Spatial and temporal variation characteristics of heatwaves in recent decades over China. Remote Sens. 13 (19), 3824. https://doi.org/10.3390/rs13193824.

Liu, J., Ren, Y., Tao, H., Shalamzari, M.J., 2021b. Spatial and temporal variation characteristics of heatwaves in recent decades over China. Remote Sens. 13 (19). https://doi.org/10.3390/rs13193824.

Liu, S., Li, M., Liu, Y., Ni, F., Zhou, C., Tabak, B.M., 2021. How and when factors of agricultural contribution influence urbanization: a historical analysis of Tibet. Discrete Dyn. Nat. Soc. 2021, 1–15. https://doi.org/10.1155/2021/7255274.

Lobell, D.B., Sibley, A., Ivan Ortiz-Monasterio, J., 2012. Extreme heat effects on wheat senescence in India. Nat. Clim. Chang. 2 (3), 186–189. https://doi.org/10.1038/Nclimate1356.

Lu, T., Wu, N., Luo, P., 2009. Sedentarization of tibetan nomads. Conserv. Biol. 23 (5), 1074. https://doi.org/10.1111/j.1523-1739.2009.01312.x.

Luo, L., Duan, Q., Wang, L., Zhao, W., Zhuang, Y., 2020. Increased human pressures on the alpine ecosystem along the Qinghai-Tibet railway. Reg. Environ. Chang. 20 (1). https://doi.org/10.1007/s10113-020-01616-7.

Luo, L., Sun, W., Han, Y., Zhang, W., Liu, C., Yin, S., 2020. Importance evaluation based on random forest algorithms: insights into the relationship between negative air ions variability and environmental factors in urban green spaces. Atmosphere 11 (7), 706. https://doi.org/10.3390/atmos11070706.

Luo, M., Lau, N.-C., 2019. Amplifying effect of ENSO on heat waves in China. Clim. Dyn. 52 (5), 3277–3289. https://doi.org/10.1007/s00382-018-4322-0.

Lyamani, H., Olmo, F., Alcántara, A., Alados-Arboledas, L., 2006. Atmospheric aerosols during the 2003 heat wave in southeastern Spain II: microphysical columnar properties and radiative forcing. Atmos. Environ. 40 (33), 6465–6476. https://doi.org/10.1016/j.atmosenv.2006.04.047.

Mann, H.B., 1945. Nonparametric tests against trend. Econometrica 13 (3), 245–259. https://doi.org/10.2307/1907187.

Mills, K.E., Pershing, A.J., Brown, C.J., Chen, Y., Chiang, F.-S., Holland, D.S., Lehuta, S., Nye, J.A., Sun, J.C., Thomas, A.C., 2013. Fisheries management in a changing climate: lessons from the 2012 ocean heat wave in the Northwest Atlantic. Oceanography 26 (2), 191–195. https://doi.org/10.5670/oceanog.2013.27.

Miralles, D.G., Teuling, A.J., Van Heerwaarden, C.C., Vilà-Guerau de Arellano, J., 2014. Mega-heatwave temperatures due to combined soil desiccation and atmospheric heat accumulation. Nat. Geosci. 7 (5), 345–349. https://doi.org/10.1038/Ngeo2141.

Mondal, S., Mishra, A.K., 2021. Complex networks reveal heatwave patterns and propagations over the USA. Geophys. Res. Lett. 48 (2), e2020GL090411. https://doi.org/10.1029/2020GL090411.

Mukherjee, S., Mishra, A.K., 2021. Increase in compound drought and heatwaves in a warming world. Geophys. Res. Lett. 48 (1), e2020GL090617. https://doi.org/10.1029/2020GL090617.

Perkins-Kirkpatrick, S.E., Fischer, E.M., Angélil, O., Gibson, P.B., 2017. The influence of internal climate variability on heatwave frequency trends. Environ. Res. Lett. 12 (4), 044005. https://doi.org/10.1088/1748-9326/aa63fe.

Perkins, S.E., Alexander, L.V., 2013. On the measurement of heat waves. J. Clim. 26 (13), 4500–4517. https://doi.org/10.1175/jcli-d-12-00383.1.

Perkins, S.E., Alexander, L.V., Nairn, J.R., 2012. Increasing frequency, intensity and duration of observed global heatwaves and warm spells. Geophys. Res. Lett. 39. https://doi.org/10.1029/2012gl053361.

Piao, S., Ciais, P., Huang, Y., Shen, Z., Peng, S., Li, J., Zhou, L., Liu, H., Ma, Y., Ding, Y., 2010. The impacts of climate change on water resources and agriculture in China. Nature 467 (7311), 43–51. https://doi.org/10.1038/nature09364.

Pogačar, T., Casanueva, A., Kozjek, K., Ciuha, U., Mekjavić, I.B., Kajfež Bogataj, L., Črepinšek, Z., 2018. The effect of hot days on occupational heat stress in the manufacturing industry: implications for workers' well-being and productivity. Int. J. Biometeorol. 62 (7), 1251–1264. https://doi.org/10.1007/s00484-018-1530-6.

Qi, W., Liu, S., Zhou, L., 2020. Regional differentiation of population in tibetan plateau: insight from the "Hu Line". Acta Geograph. Sin. 75 (2), 255–267. https://doi.org/10.11821/dlxb202002004.

Reichle, R.H., Draper, C.S., Liu, Q., Girotto, M., Mahanama, S.P.P., Koster, R.D., De Lannoy, G.J.M., 2017. Assessment of MERRA-2 land surface hydrology estimates. J. Clim. 30 (8), 2937–2960. https://doi.org/10.1175/jcli-d-16-0720.1.

Robine, J.-M., Cheung, S.L.K., Le Roy, S., Van Oyen, H., Griffiths, C., Michel, J.-P., Herrmann, F.R., 2008. Death toll exceeded 70,000 in Europe during the summer of 2003. C.R. Biol. 331 (2), 171–178. https://doi.org/10.1016/j.crvi.2007.12.001.

Rohini, P., Rajeevan, M., Srivastava, A., 2016. On the variability and increasing trends of heat waves over India. Sci. Rep. 6 (1), 1–9. https://doi.org/10.1038/srep26153.

Sen, P.K., 1968. Estimates of the regression coefficient based on Kendall's tau. J. Am. Stat. Assoc. 63 (324), 1379–1389. https://doi.org/10.1080/01621459.1968.10480934.

Seo, Y.-W., Ha, K.-J., Park, T.-W., 2021. Feedback attribution to dry heatwaves over East Asia. Environ. Res. Lett. 16 (6), 064003. https://doi.org/10.1088/1748-9326/abf18f.

Sharifi, E., Steinacker, R., Saghafian, B., 2018. Multi time-scale evaluation of high-resolution satellite-based precipitation products over northeast of Austria. Atmos. Res. 206, 46–63. https://doi.org/10.1016/j.atmosres.2018.02.020.

Shen, Z., Zhang, Q., Singh, V.P., Sun, P., He, C., Cheng, C., 2021. Station-based non-linear regression downscaling approach: a new monthly precipitation downscaling technique. Int. J. Climatol. 41 (13), 5879–5898. https://doi.org/10.1002/joc.7158.

Shi, Z., Jia, G., Zhou, Y., Xu, X., Jiang, Y., 2021. Amplified intensity and duration of heatwaves by concurrent droughts in China. Atmos. Res. 261. https://doi.org/10.1016/j.atmosres.2021.105743.

Stegehuis, A., Vogel, M., Vautard, R., Ciais, P., Teuling, A., Seneviratne, S., 2021. Early summer soil moisture contribution to Western European summer warming. J. Geophys. Res.: Atmos. 126 (17), e2021JD034646. https://doi.org/10.1029/2021JD034646.

Sun, X., Sun, Q., Zhou, X., Li, X., Yang, M., Yu, A., Geng, F., 2014. Heat wave impact on mortality in Pudong new area, China in 2013. Sci. Total Environ. 493, 789–794. https://doi.org/10.1016/j.scitotenv.2014.06.042.

Theil, H., 1992. A rank-invariant method of linear and polynomial regression analysis. Henri Theil's Contributions to Economics and Econometrics. Springer, pp. 345–381 https://doi.org/10.1007/978-94-011-2546-8_20.

Vautard, R., van Aalst, M., Boucher, O., Drouin, A., Haustein, K., Kreienkamp, F., Van Oldenborgh, G.J., Otto, F.E., Ribes, A., Robin, Y., 2020. Human contribution to the record-breaking june and july 2019 heatwaves in Western Europe. Environ. Res. Lett. 15 (9), 094077. https://doi.org/10.1088/1748-9326/aba3d4.

Vijverberg, S., Coumou, D., 2022. The role of the Pacific decadal oscillation and ocean-atmosphere interactions in driving US temperature predictability. npj Clim. Atmos. Sci. 5 (1). https://doi.org/10.1038/s41612-022-00237-7.

Wang, X., Qiu, B., Li, W., Zhang, Q., 2019. Impacts of drought and heatwave on the terrestrial ecosystem in China as revealed by satellite solar-induced chlorophyll fluorescence. Sci. Total Environ. 693, 133627. https://doi.org/10.1016/j.scitotenv.2019.133627.

Wang, X., Wen, Q., Wu, Y., 2007. Penalized maximal t test for detecting undocumented mean change in climate data series. J. Appl. Meteorol. Climatol. 46 (6), 916–931. https://doi.org/10.1175/jam2504.1.

Wang, G., Zhang, Q., Luo, M., Singh, V.P., Xu, C., 2022. Fractional contribution of global warming and regional urbanization to intensifying regional heatwaves across Eurasia. Clim. Dyn., 1–17 https://doi.org/10.1007/s00382-021-06054-7.

Wang, X., Zhou, W., Wang, D., Wang, C., 2013. The impacts of the summer asian jet stream biases on surface air temperature in mid-eastern China in IPCC AR4 models. Int. J. Climatol. 33 (2), 265–276. https://doi.org/10.1002/joc.3419.

Wang, Y.Y., Lyu, R., Xie, X., Meng, Z., Huang, M.J., Wu, J.S., Mu, H.Z., Yu, Q.R., He, Q.S., Cheng, T.T., 2020. Retrieval of gridded aerosol direct radiative forcing based on multiplatform datasets. Atmos. Meas. Tech. 13 (2), 575–592. https://doi.org/10.5194/amt-13-575-2020.

Wild, M., Ohmura, A., Makowski, K., 2007. Impact of global dimming and brightening on global warming. Geophys. Res. Lett. 34 (4), 4. https://doi.org/10.1029/2006gl028031.

Wondmagegn, B.Y., Xiang, J.J., Dear, K., Williams, S., Hansen, A., Pisaniello, D., Nitschke, M., Nairn, J., Scalley, B., Varghese, B.M., Xiao, A., Jian, L., Tong, M., Bambrick, H., Karnon, J., Bi, P., 2021. Impact of heatwave intensity using excess heat factor on emergency department presentations and related healthcare costs in Adelaide. South Australia. Sci. Total Environ. 781. https://doi.org/10.1016/j.scitotenv.2021.146815.

Wu, Z., Jiang, Z., Li, J., Zhong, S., Wang, L., 2012. Possible association of the western tibetan plateau snow cover with the decadal to interdecadal variations of northern China heatwave frequency. Clim. Dyn. 39 (9), 2393–2402. https://doi.org/10.1007/s00382-012-1439-4.

Wu, X., Wang, L., Yao, R., Luo, M., Li, X., 2021. Identifying the dominant driving factors of heat waves in the North China Plain. Atmos. Res. 252, 105458. https://doi.org/10.1016/j.atmosres.2021.105458.

Xia, Y., Li, Y., Guan, D., Tinoco, D.M., Xia, J., Yan, Z., Yang, J., Liu, Q., Huo, H., 2018. Assessment of the economic impacts of heat waves: a case study of Nanjing. China. J. Cleaner Prod. 171, 811–819. https://doi.org/10.1016/j.jclepro.2017.10.069.

Xiong, J., Wang, Z., Lai, C., Liao, Y., Wu, X., 2020. Spatiotemporal variability of sunshine duration and influential climatic factors in mainland China during 1959–2017. Int. J. Climatol. 40 (15), 6282–6300. https://doi.org/10.1002/joc.6580.

Xu, W., Li, Q., Wang, X.L., Yang, S., Cao, L., Feng, Y., 2013. Homogenization of chinese daily surface air temperatures and analysis of trends in the extreme temperature indices. J. Geophys. Res. Atmos. 118 (17), 9708–9720. https://doi.org/10.1002/jgrd.50791.

Xu, Z., Cheng, J., Hu, W., Tong, S., 2018. Heatwave and health events: a systematic evaluation of different temperature indicators, heatwave intensities and durations. Sci. Total Environ. 630, 679–689. https://doi.org/10.1016/j.scitotenv.2018.02.268.

Xu, Z., FitzGerald, G., Guo, Y., Jalaludin, B., Tong, S., 2016. Impact of heatwave on mortality under different heatwave definitions: a systematic review and meta-analysis. Environ. Int. 89–90, 193–203. https://doi.org/10.1016/j.envint.2016.02.007.

Xu, Z., Tong, S., Cheng, J., Zhang, Y., Wang, N., Zhang, Y., Hayixibayi, A., Hu, W., 2019. Heatwaves, hospitalizations for Alzheimer's disease, and postdischarge deaths: a population-based cohort study. Environ. Res. 178, 108714. https://doi.org/10.1016/j.envres.2019.108714.

Yamashita, T., Yamashita, K., Kamimura, R., 2007. A stepwise AIC method for variable selection in linear regression. Commun. Stat. Theory Methods 36 (13), 2395–2403. https://doi.org/10.1080/03610920701215639.

Yang, J., Huang, X., 2021. The 30 m annual land cover dataset and its dynamics in China from 1990 to 2019. Earth Syst. Sci. Data 13 (8), 3907–3925. https://doi.org/10.5194/essd-13-3907-2021.

Ye, D., Yin, J., Chen, Z., Zheng, Y., Wu, R., 2014. Spatial and temporal variations of heat waves in China from 1961 to 2010. Adv. Clim. Chang. Res. 5 (2), 66–73. https://doi.org/10.3724/sp.j.1248.2014.066.

Yu, L., Leng, G., 2022. Identifying the paths and contributions of climate impacts on the variation in land surface albedo over the Arctic. Agric. For. Meteorol. 313, 108772. https://doi.org/10.1016/j.agrformet.2021.108772.

Yu, L., Leng, G., Python, A., Peng, J., 2021. A comprehensive evaluation of latest GPM IMERG V06 early, late and final precipitation products across China. Remote Sens. 13 (6), 1208. https://doi.org/10.3390/rs13061208.

Yu, Y., Shao, Q., Lin, Z., Kang, I.-S., 2021. Characteristics analysis and synoptic features of event-based regional heatwaves over China. J. Geophys. Res. Atmos. 126 (2). https://doi.org/10.1029/2020jd033865.

Yue, S., 2002. Applicability of prewhitening to eliminate the influence of serial correlation on the Mann-Kendall test. Water Resour. Res. https://doi.org/10.1029/2001WR000861.

Zhao, L., Lee, X., Smith, R.B., Oleson, K., 2014. Strong contributions of local background climate to urban heat islands. Nature 511 (7508), 216–219. https://doi.org/10.1038/nature13462.

Zhang, Q., Wu, Z., Yu, H., Zhu, X., Shen, Z., 2020. Variable urbanization warming effects across metropolitans of China and relevant driving factors. Remote Sens. 12 (9), 1500. https://doi.org/10.3390/rs12091500.

Zheng, J., Fan, J., Zhang, F., 2019. Spatiotemporal trends of temperature and precipitation extremes across contrasting climatic zones of China during 1956–2015. Theor. Appl. Climatol. 138 (3–4), 1877–1897. https://doi.org/10.1007/s00704-019-02942-5.

Zhou, Y., Wu, Z., 2016a. Possible impacts of mega-El Nino/Southern oscillation and Atlantic multidecadal oscillation on Eurasian heatwave frequency variability. Q. J. R. Meteorol. Soc. 142 (697), 1647–1661. https://doi.org/10.1002/qj.2759.

Zhou, X.F., Chen, H., 2018. Impact of urbanization-related land use land cover changes and urban morphology changes on the urban heat island phenomenon. Sci. Total Environ. 635, 1467–1476. https://doi.org/10.1016/j.scitotenv.2018.04.091.

Zhou, Z.G., Lin, A.W., Wang, L.C., Qin, W.M., Zhong, Y., He, L.J., 2020. Trends in downward surface shortwave radiation from multi-source data over China during 1984–2015. Int. J. Climatol. 40 (7), 3467–3485. https://doi.org/10.1002/joc.6408.